Available online at www.sciencedirect.com
SCIENCE DIRECT®

Polymer 45 (2004) 3099–3110

polymer

www.elsevier.com/locate/polymer

Coarse-grained simulation of polymer translocation through an artificial nanopore

Yves Lansac[a,*], Prabal K. Maiti[a], Matthew A. Glaser[b]

[a]Materials and Process Simulation Center, Division of Chemistry and Chemical Engineering, California Institute of Technology, Pasadena, CA 91125, USA
[b]Condensed Matter Laboratory, Ferroelectric Liquid Crystal Materials Research Center, Department of Physics, University of Colorado, Boulder, CO 80309, USA

Received 6 September 2003; received in revised form 6 February 2004; accepted 10 February 2004

Abstract

The translocation of a macromolecule through a nanometer-sized pore is an interesting process with important applications in the development of biosensors for single-molecule analysis and in drug delivery and gene therapy. We have carried out a molecular dynamics simulation study of electrophoretic translocation of a generic charged polymer through an artificial nanopore as a first step to explore the feasibility of semiconductor-based nanopore devices for ultra-fast sequencing of biological macromolecules. The polymer is represented by a simple bead-spring model designed to yield an appropriate coarse-grained description of a generic linear hydrophilic polymer in solution. A detailed analysis of single translocation event is presented to assess whether the passage of individual ions through the pore can be detected by measuring variations in electrostatic potential during polymer translocation. We find that it is possible to identify single events corresponding to the passage of individual counterions and the polymer chain as a whole, through the pore. However, discrimination of individual ions on the polymer chain based on variations in electrostatic potential is problematic. Several distinct stages in the translocation process are identified, characterized by changes in polymer conformation and by variations in the magnitude and direction of the internal electric field induced by the fluctuating charge distribution. The dependence of the condensed fraction of counterions on Bjerrum length leads to significant changes in polymer conformation, which profoundly affect the dynamics of electrophoresis and translocation.

Keywords: Polyelectrolyte; Translocation; Nanopore

---

1. Introduction

In 1993, Branton and Deamer demonstrated that DNA could be threaded through a biological pore and that, by measuring the variations in the accompanying ionic current, information about DNA secondary structure could be obtained [1]. Although these results were very promising, little progress has been made towards actual sequencing of DNA due to the limited voltage range that can be applied across a biological pore and the difficulty in measuring the current variations, because the shot noise is comparable to the expected signal [2]. An alternative approach currently under investigation [2] consists in using the new capabilities in nanoscale semiconductor technology to create a more optimized pore geometry. A device consisting of a nanometer-sized pore in a thin silicon membrane with vertical transistors positioned along the wall of the pore may, in principle, be able to detect charges passing through the pore by measuring image charges in the transistor. By reducing the noise and maximizing the charge and current sensitivity, the proposed geometry may achieve DNA sequencing with order of magnitude improvements in speed and cost and minimal pre- and post-measurement procedures compared to current sequencing techniques. The expected scientific and therapeutic benefits will be dramatic, for example enabling rapid routine screening for treatable genetic disorders.

Although an empirical approach based on trial and error can lead to some progress in the fabrication of such devices, a fundamental physical understanding of the delicate interplay between the physico-chemical behavior of the macromolecule in solution and the interaction with the confining geometry induced by the solid surface of the pore

---

[*] Corresponding author. Tel.: +1-626-395-8137; fax: +1-626-585-0918.
E-mail address: lansac@wag.caltech.edu (Y. Lansac).

0032-3861/$ - see front matter © 2004 Elsevier Ltd. All rights reserved.
doi:10.1016/j.polymer.2004.02.040

is highly desirable. Molecular modeling is a powerful tool to investigate the collective behavior of systems resulting from the complex interactions between their individual components. Such an approach may allow us to gain insight into the phenomena of driven polymer translocation through a nanometer-scale pore from both an applied and a fundamental point of view. From an applied point of view, we can assess the feasibility of sensing and identifying individual nucleotides, to aid in the design of semiconductor-based devices and in the interpretation of the experimental measurements. In order to achieve this goal, atomistic modeling using high accuracy molecular models must be used to represent the properties of single stranded DNA, aqueous solution and substrate quantitatively. With this prerequisite, it is possible to study the local structure, conformation, and short time dynamics of single-stranded DNA in confined geometries, and to investigate the translocation of ions and counterions across the channel as a function of the pore diameter and shape and of the magnitude of the potential difference applied. From a more fundamental point of view, it is of interest to study the mechanism of polymer translocation and the behavior of polyelectrolytes in confined geometries. This is of relevance to the process of pore entry, including studies of the role of counterion charge density gradients and of the role played by hydrodynamic effects. A better understanding of this process can guide the design of pore geometries that effectively steer DNA molecules toward the pore.

Polymer translocation involves traversal of a free energy barrier arising from several distinct physical effects, including loss of conformational entropy of the macromolecule upon traversal (an entropic barrier) [3–5], mismatch in dielectric constant between the aqueous solution and the silicon pore (an electrostatic barrier) [6] and specific interactions of the macromolecule with the pore surface (an enthalpic barrier) [5,7]. Although the actual process of translocation is complicated by many biological and physical factors, a simple model in which an idealized linear charged polymer chain translocates through an artificial pore provides a useful framework to investigate the basic features of the threading process in three dimensions in the presence of an explicit solvent. In this study, we use a coarse-grained approach [8–11], in which groups of atoms are represented by single interaction sites, to capture many of the essential physical features of the system. We use an explicit coarse-grained model to represent the solvent in order to take into account hydrodynamic effects, which could play an important role in the electrophoretic transport of a polymer chain (e.g. backflow effects) as well as in the polymer/pore interactions (e.g. confined geometry effects). By dramatically decreasing the number of degrees of freedom present, this model can engender improved basic qualitative understanding of field-driven polymer translocation over long length and time scales. Note that we do not focus here on the statistics of polymer translocation events, which is difficult to study by direct molecular dynamics simulation due to the presence of an explicit solvent. We focus on the qualitative behavior of a polylectrolyte in free and constraint geometry, the influence of an external field and the possible discrimination between monomers during polymer translocation based on their electrostatic signature.

The remainder of this article is organized as follows: in Section 2, we define the interaction potential used in this study, the parametrization used to represent a generic charged polymer chain in solution, and the simulation methodology. In Section 3 we present results obtained in the translocation process and the influence of Bjerrum length and external electric field on the conformational characteristics of the polymer. Finally, conclusions drawn from this study as well as future research directions are discussed in Section 4.

2. Methodology

2.1. Interaction potential

We study the translocation of a single negatively charged polymer chain in a solvent containing counterions. Each molecule in this three-species mixture is represented as a set of spherical interaction sites. A coarse-grained approach in which groups of atoms are represented by single interaction sites is used in order to reduce the computational cost and to enable the study of the translocation process on long timescales.

We choose a simple interaction potential of the form: $U(\mathbf{r}^N) = U_{\mathrm{str}} + U_{\mathrm{vdw}} + U_{\mathrm{coul}} + U_{\mathrm{ext}} + U_{\mathrm{wall}}$. The first term describes intramolecular valence interactions, with U_{str} representing bond stretching interactions. We chose to model the charged polymer as a flexible chain without bond angle bending or dihedral torsion interactions. It must be pointed out that the chain is not fully flexible due to intramolecular van der Waals and Coulombic interactions between second and more distant neighbors. The last four terms describe non-bonded interactions, with U_{vdw}, U_{coul}, U_{ext} and U_{wall} representing van der Waals, Coulombic, external electric field, and molecular site–substrate interactions, respectively. The pore is defined as a cylindrical channel (with axis along the z direction) in a solid substrate, which is treated as a smooth van der Waals surface, and the external electric field E driving polymer translocation is in the $+z$ direction. These contributions to the total potential are defined as:

$$U_{\mathrm{str}} = \sum_{\substack{\mathrm{bonds}\\ ij}} \frac{1}{2} k_r (r_{ij} - r_{\mathrm{eq}})^2 \tag{1}$$

$$U_{\mathrm{vdw}} = {\sum_{i<j}}' 4\epsilon_{ij}\left[\left(\frac{\sigma_{ij}}{r_{ij}}\right)^{12} - \left(\frac{\sigma_{ij}}{r_{ij}}\right)^{6}\right] \tag{2}$$

$$U_{\text{coul}} = \sum_{i<j}{}' \frac{q_i q_j}{r_{ij}} \tag{3}$$

$$U_{\text{ext}} = \sum_i E q_i z_i \tag{4}$$

$$U_{\text{wall}} = \sum_i 4\epsilon_{iw}\left[\left(\frac{\sigma_{iw}}{r_{iw}}\right)^{12} - \left(\frac{\sigma_{iw}}{r_{iw}}\right)^{6}\right] \tag{5}$$

The primes on the sums in Eqs. (2) and (3) indicate that nearest-neighbor intramolecular non-bonded interactions are excluded from the sums. The distance r_{ij} between sites i and j is defined as $r_{ij} = |\mathbf{r}_{ij}| = |\mathbf{r}_j - \mathbf{r}_i|$ where $\mathbf{r}_i$ is the position of site i and z_i its vertical component.

The remaining step in building the molecular model is fixing the interaction parameters. These parameters need to be provided for every distinct combination of site types. In Section 2.2, the site types and the interaction parameters used in the case of the coarse-grained model will be specified.

2.2. Parametrization of the coarse-grained model

An appropriate parametrization of the coarse-grained molecular model is obtained via an approximate mapping from the corresponding physical system. Even if our study focuses only on an idealized generic polyelectrolyte system, it is useful to identify the solvent model to a rough analog of water in order to get an idea of the order of magnitude of the important quantities controlling the translocation process. Solvent molecules are treated as point van der Waals (Lennard–Jones) interaction sites, with the Lennard–Jones (LJ) parameters determined from a 'corresponding states' mapping of the triple point of water onto that of the LJ system [12] yielding $\sigma_{\text{sol}} = 0.29$ nm and $\epsilon_{\text{sol}} = 0.79$ kcal/mol. These values are taken as the unit of length σ_0 and the unit of energy ϵ_0. The mass of a single water molecule is the unit of mass, $m_0 = 18$ a.u. Using these values, a unit of time $t_0 = \sqrt{m_0\sigma_0^2/\epsilon_0} \simeq 7\times 10^{-10}$ s, a unit of charge $q_0 = \sqrt{\epsilon_0\sigma_0} \simeq e/12$, and a unit of electric field $E_0 = \epsilon_0/(q_0\sigma_0) \simeq 1400$ V/μm are defined, where e is the magnitude of the electron charge.

We model a generic negatively charged polymer and set the concentration of positively-charged counterions such that the system is neutral overall. The counterions are treated as point interaction sites with the same LJ parameters as water and with a reduced charge $q_{\text{counter}} = \alpha q_0$. We have investigated systems with $\alpha = 1.2$, 2.4 and 6 corresponding to a charge $q_{\text{counter}} = e/10$, $e/5$ and $e/2$. These values have been chosen in order to take into account the dielectric screening effects from the surrounding solvent (i.e. the apparent weaker electrostatic interaction between two charges in solution as compared to in vacuum) in an approximate way [13]. In aqueous solution, the polymer–polymer and polymer–counterions electrostatic interactions are affected by the solvent polarization and a simple approximation to reproduce the electrostatic potential in solution is to reparametrize the partial atomic charges in such a way that simple Coulomb potential can still be used. This effect can be achieved by scaling down the charges q_i and q_j carried by phosphate groups and counterions with scaling factors λ_i and λ_j such that $E_{\text{coul}} = (q_i/\lambda_i)\times(q_j/\lambda_j)\times(1/r_{ij})$. For simplicity, the mass of counterions is set equal to the mass of solvent molecules.

The polymer chain consists of alternating charged and non-charged groups. Each group is represented by a van der Waals point interaction site with van der Waals parameters $\sigma_{\text{poly}} = 2\sigma_0$ and $\epsilon_{\text{poly}} = \epsilon_0$. The charged sites carry reduced electric charge $q_{\text{poly}} = -q_{\text{counter}}$. We study an overall hydrophilic polymer chain and therefore, for simplicity, the same generic van der Waals parameters have been used to describe both solvent–charged group and solvent–non-charged group interactions.

The bond stretching parameters are set to the following generic values: $r_{\text{eq}} = \sigma_0$ and $k_r = 24$ kcal/mol. The polymer chain is quite flexible although not fully flexible due to the van der Waals and Coulombic interactions between second and more distant neighbors. The masses of both charged and non-charged sites are set to $5m_0$. Geometrical combination rules for σ and ϵ were applied to parametrize the LJ interactions between unlike species.

The pore is defined as a cylindrical channel in a solid substrate, which is treated as a smooth van der Waals surface, the atomic sites interacting with the nearest point on the surface of the pore or substrate. For simplicity, the LJ parameters of the wall sites are the same as those of the solvent. The diameter of the pore is $d_{\text{pore}} = 5\sigma_0$ with a length $l_{\text{pore}} = 2d_{\text{pore}}$. Within the framework of this simple pore model, dielectric self-energy [14] which arises when an ion moves through a relatively narrow channel and which is known to affect the dynamics of ions permeation in biological channels has been neglected. The diameter of the pore is 2.5 times larger than that of the polymer in order to accommodate both the polymer chain and at most one solvation sphere. Reduced variables defined in this subsection are used in the remainder of this article.

2.3. Simulation methodology

We carry out NVT (constant particle number, volume, and temperature) molecular dynamics simulations of a single charged polymer in solution, under an external field, with periodic boundary conditions. The unit cell contains a reservoir separated by an impenetrable substrate of thickness l_{pore} and surface area equal to the lateral dimension of the unit cell, and containing a cylindrical hole (nanopore) of diameter d_{pore} (Fig. 1).

The chain consists of 40 sites, alternating between charged and non-charged groups, and the initial state is built such that the charged polymer is in the reservoir outside the pore cavity. The system contains, in addition to the polymer, 6000 solvent molecules and 20 counterions with initial

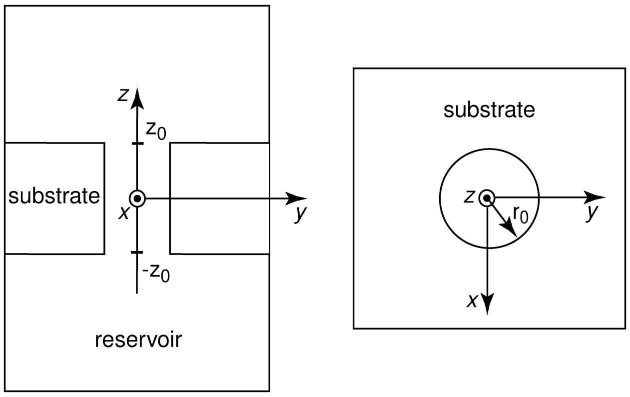

Fig. 1. Side view (left) and top view (right) of the simulated system, comprised of a reservoir with a substrate containing a nanopore of radius r_0 and length $2z_0$.

positions chosen randomly in the unit cell. The simulation was carried out at a reduced density $\rho^* = 0.85$ and a reduced temperature $T^* = k_B T/\epsilon_0 = 0.75$, corresponding to the dense fluid phase of a LJ system. The applied external electric field of magnitude $E^* = E/E_0 = 0.5$, corresponding to a field $E = 709$ V/μm, is turned on after an initial equilibration run of duration $t^* = 500$. Such a large field is used in the present study in order to ensure that field-driven translocation occurs on a time scale accessible to simulations.

A single-timestep velocity–Verlet MD integration scheme was used to integrate the equations of motion with a timestep $\delta t = 2.5 \times 10^{-3}$, and the weak-coupling algorithm of Berendsen et al. [15] was used to maintain constant temperature. All LJ interactions were truncated at 2.5 σ_0 and no long-range corrections were applied. Long-range Coulomb interactions are evaluated to high accuracy using the particle-mesh Ewald (PME) method [16,17]. The PME technique, which is derived from the conventional Ewald method [18,19], makes use of the FFT to efficiently compute the long-range part of the electrostatic interaction. In this study we used a highly optimized version of the PME with a relative accuracy of 10^{-4}.

We have carried out three simulations of systems with reduced charge magnitude $q^* = 1.2$, 2.4 and 6.0 for durations of 4.2×10^6, 3.0×10^6 and 5.2×10^6 timesteps, respectively.

3. Results

The translocation process consists of three distinct stages: in the first stage, the polymer drifts through the reservoir, driven by the external electric field. In the second stage, the polymer is pushed against the lower substrate surface and behaves like a two-dimensional chain wandering in search of the pore entrance. In the third stage, the polymer finds the entrance to the pore and translocation takes place.

Due to the relatively small system size, the time spent by the polymer in the second stage is small compared to that in the two other stages. We first study the electrophoresis of the charged polymer in the reservoir, then the kinetics of the translocation process and the possibility of identifying individual ions passing through the pore from the electrostatic signal produced.

3.1. Electrophoresis in the reservoir

Electrophoresis is a complex process dependent on the electrophoretic friction coefficient [20]. This coefficient arises both from the macroion/solvent interactions, comprising the monomer/solvent interaction (the intrinsic friction) and from hydrodynamic interactions between monomer pairs, and from macroion/ion interactions. Since the macroion is negatively charged, it is surrounded by an oppositely charged liquid atmosphere [21]. The force acting on the ions in the atmosphere is transmitted to the solvent, and therefore the atmospheric liquid behaves as a charged volume. Under an applied electric field, this charged liquid is subject to a volume force in the opposite direction from the drift velocity of the macroion. The macroion thus moves against a local hydrodynamic flow that slows its motion (relative to a hypothetical drift without the charged liquid). In addition, the electric field deforms the charged volume, increasing the atmospheric charge density at the end of the polymer opposite to the end, which drifts and decreasing ahead of the macroion. This effect induces an internal field (often referred in the literature as the relaxation field, or more accurately, the asymmetry field) opposing the external electric field, which also slows down the macroion motion.

Counterion condensation is in large part responsible for the structure and behavior of the liquid atmosphere and, as recognized in the late 1960s independently by Oosawa and Manning [22,23], plays a crucial role in the strong attractive interaction that acts between highly charged macroions such as DNA, leading to significant conformational changes. Counterion condensation results in a competition between Coulombic energy and entropy in minimizing the free energy of an aqueous solution containing mobile ions in the vicinity of an isolated macroion. For rodlike objects, whether the entropy or the Coulombic attraction dominates depends on the charge density of the macroion measured in terms of the Bjerrum length $\lambda_B = q^2/k_B T$, defined as the distance at which the Coulombic interaction between two charges is equal to the thermal energy $k_B T$. Counterion condensation occurs when the distance b between charges on the macroion is small enough for the dimensionless parameter $\Gamma = \lambda_B/b$ (the Manning parameter) to exceed unity. With the reduced units introduced in Section 2, a reduced Bjerrum length $\lambda_B^* = q^{*2}/T^*$ is defined. In the present model, the distance between two charges is $b = 2\sigma_0$, leading to a Manning parameter $\Gamma = q^{*2}/2T^*$. Values for λ_B^* and Γ are listed in Table 1 for the systems with reduced charge $q^* = 1.2$, 2.4, 6.0. At the reduced temperature chosen in this study, Coulombic interactions dominate over

Table 1
Electrostatic and conformational properties of the simulated systems

	$q^* = 1.2$	$q^* = 2.4$	$q^* = 6.0$
λ_B^*	1.92	7.68	48.0
Γ	0.96	3.8	24.0
Number of condensed counterions ($E^* = 0$)	2.347 ± 0.158 ($r_c^* = 1.8$) 2.897 ± 0.263 ($r_c^* = 2.0$) 10.174 ± 2.266 ($r_c^* = 6.0$)	4.761 ± 0.712 (1.8) 5.706 ± 1.074 (2.0) 12.358 ± 2.428 (6.0)	11.785 ± 1.897 (1.8) 12.726 ± 2.044 (2.0) 16.866 ± 1.648 (6.0)
Number of condensed counterions of ($E^* = 0.5$)	0.283 ± 0.138 ($r_c^* = 1.8$) 0.268 ± 0.149 ($r_c^* = 2.0$) 1.567 ± 0.494 ($r_c^* = 6.0$)	3.029 ± 0.902 (1.8) 3.623 ± 1.265 (2.0) 10.404 ± 3.158 (6.0)	14.254 ± 0.165 (1.8) 14.510 ± 0.079 (2.0) 18.026 ± 0.049 (6.0)
$\langle R_g^2 \rangle$ ($E^* = 0$)	23.030 ± 1.375	25.789 ± 1.459	20.202 ± 1.008
$\langle R_g^2 \rangle$ ($E^* = 0.5$)	60.007 ± 2.716	60.837 ± 7.157	13.961 ± 0.279

the thermal energy for $q^* = 6.0$ and $q^* = 2.4$ systems, which thus should exhibit strong counterion condensation. For the $q^* = 1.2$ system, $\Gamma = 0.96$, which is close enough to unity to also exhibit counterion condensation. However, in this case we expect to have a much less strongly bound counterion–macroion complex than for $q^* = 6.0$ and 2.4.

It is difficult to define an unambiguous criterion for condensation. Indeed, as pointed by Oosawa [22], for a coiled polymer chain each charged group makes a sharp and deep potential hole at its position, each linear part of the chain makes a sharp and deep potential valley along its length and the coiled chain as a whole makes a potential trough in its apparent volume. Counterions located in these three regions are considered to be condensed, with the counterions at charged group holes being localized and the counterions in the other two regions being mobile. Therefore, an estimate of the degree of condensation depends on the criterion used to discriminate between free and condensed counterions. In the present study, a counterion is said to be condensed if it is within a distance r_c^* from an ion of the polymer.

Fig. 2 shows representative configurations for the three systems both with and without applied external electric field E^*. We first study the system behavior without an external

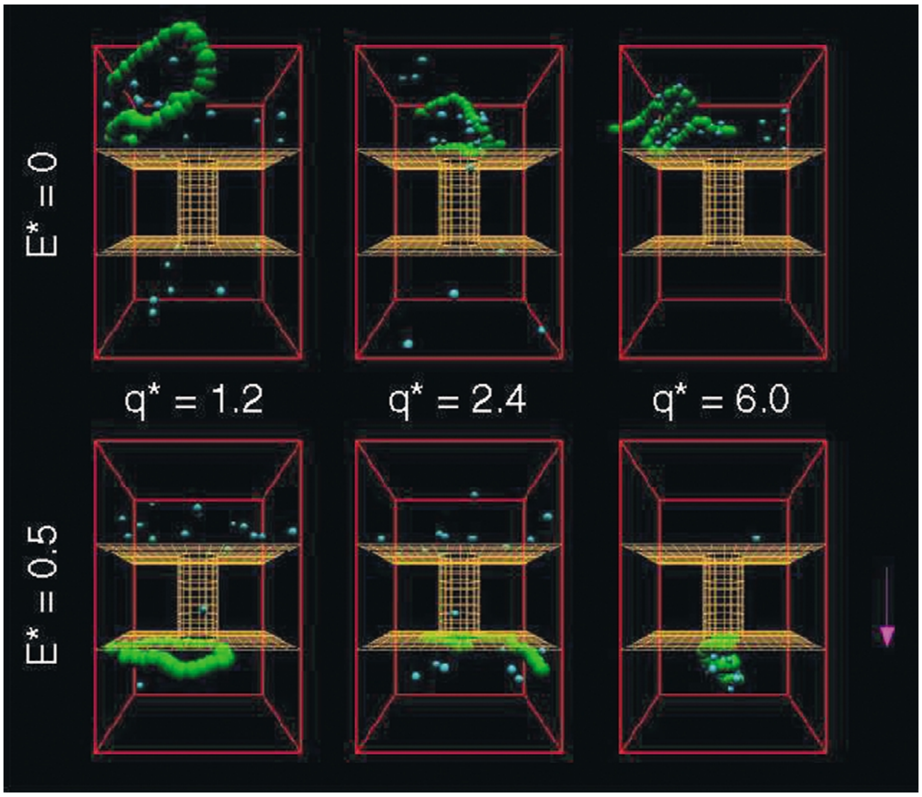

Fig. 2. Representative configurations of the three polyelectrolyte systems, without external field (top) at $t^* = 500$ and with applied electric field (bottom) at $t^* = 10,500$ for $q^* = 1.2$ and 6.0 and at $t^* = 4000$ (before translocation) for $q^* = 2.4$. For clarity, the water molecules have not been displayed.

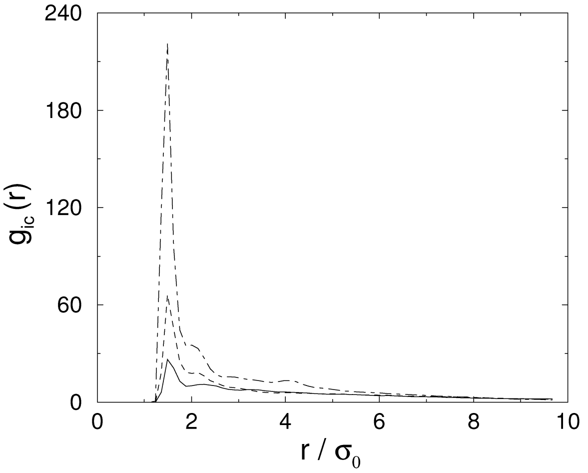

Fig. 3. Ion–counterion pair distribution function $g_{\mathrm{ic}}(r)$ for $q^* = 1.2$ (solid line), 2.4 (dashed line) and 6.0 (dot-dashed line) without external field.

applied field. The three systems exhibit counterion condensation but the nature of the resulting macroion–counterion complex varies with the magnitude of the charge. For $q^* = 6.0$, a large majority of the counterions are closely associated with the polymer chain, being mostly bound or in the narrow potential valley along the length of the chain, while for $q^* = 1.2$ the counterions are mostly located in the potential valley of the polymer chain. An intermediate situation occurs for $q^* = 2.4$. Fig. 3 shows the radial pair correlation function $g_{\mathrm{ic}}(r^*)$ between ions on the chain and counterions, for $q^* = 1.2$, 2.4 and 6.0 and $E^* = 0$. The common features exhibited are a main peak at $r^* \simeq 1.5$, corresponding to localized condensed counterions, and a shoulder around $r^* \simeq 2.0$, corresponding to mobile counterions in the narrow potential valley around the chain. The height of the main peak for $q^* = 6.0$ is roughly seven times larger than for $q^* = 1.2$ and four times larger than for $q^* = 2.4$, confirming a stronger counterion localization for larger charge magnitude. For $q^* = 1.2$, Fig. 4 shows the relative importance of longer range correlations with respect to short range correlations with the presence of secondary peaks around $r \simeq 2.3\sigma_0$ and $r \simeq 3.5\sigma_0$, indicating that a significant counterion fraction is located in the potential trough of the chain. Table 1 displays the average number of condensed counterions for the three systems for different values of r_c^* corresponding roughly to the bottom of the main peak in $g_{\mathrm{ic}}(r_c^* = 1.8)$, the shoulder ($r_c^* = 2.2$) and a value taking into account the long range correlations ($r_c^* = 6.0$).

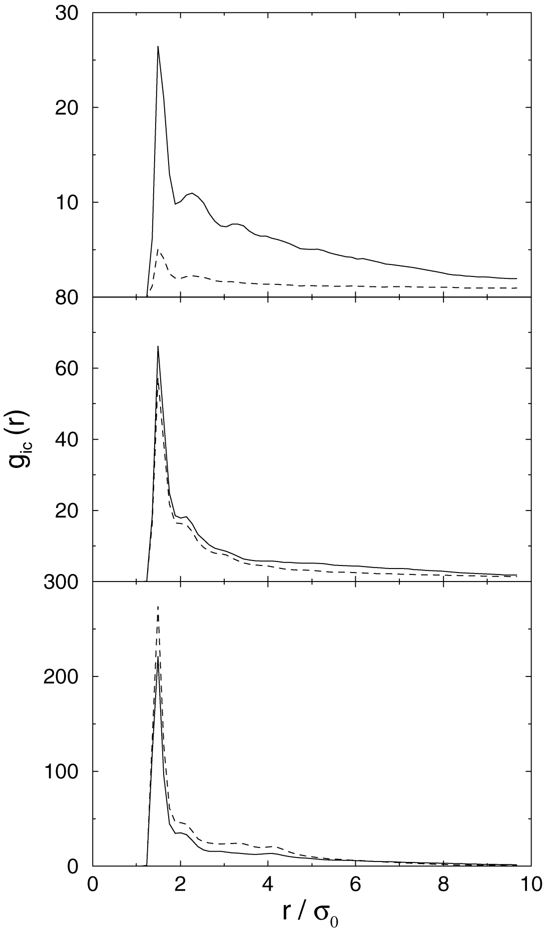

Fig. 4. Ion–counterion pair distribution function $g_{\mathrm{ic}}(r)$ for $q^* = 1.2$, 2.4 and 6.0 (from top to bottom) for $E^* = 0$ (solid line) and $E^* = 0.5$ (dashed line).

Under the applied external field, the counterions remain located very close to the macroion forming bound dipoles for $q^* = 6.0$. In addition, a conformational change occurs with the formation of a collapsed polymer structure. By contrast, for $q^* = 1.2$, the counterions are not condensed anymore (Fig. 2). The force produced by the applied external field overcomes the attractive Coulombic force and strips the counterions from the chain. As a first approximation, the reduced critical charge at which the Coulombic force exactly balances the force produced by the external field is $q_c^* = E^* \bar{r}^{*2}$ where $\bar{r}^*$ is the average reduced distance between a polymer ion and a counterion. Assuming a condensed state with all counterions bound to the polymer, the estimate $\bar{r}^* \simeq 1.5$–2.0 leads to $q_c^* = 1.125$–2.0. Thus, no counterions will be stripped from the chain for $q^* = 6.0$, while a large counterion fraction will be stripped away for $q^* = 1.2$. In the latter case, q_c^* is a lower limit since the counterions are not closely bound to the chain (see Fig. 2). A Monte Carlo simulation study of the counterion condensation on a spherical macroion has shown the same phenomenon under a strong external field [24]. With this estimate, the counterion fraction located in the potential trough of the chain will be stripped from the polymer for $q^* = 2.4$.

Fig. 4 shows the ion–counterion pair correlation function when an external electric field is applied on the systems. For $q^* = 1.2$, the magnitude of the main peak for $q^* = 1.2$ is reduced by an order of magnitude, confirming that a large counterion fraction is stripped from the chain. The electric field has a much less drastic effect on the two other systems: a small fraction of counterions are stripped from the chain for $q^* = 2.4$ while for $q^* = 6.0$, the field enhances slightly

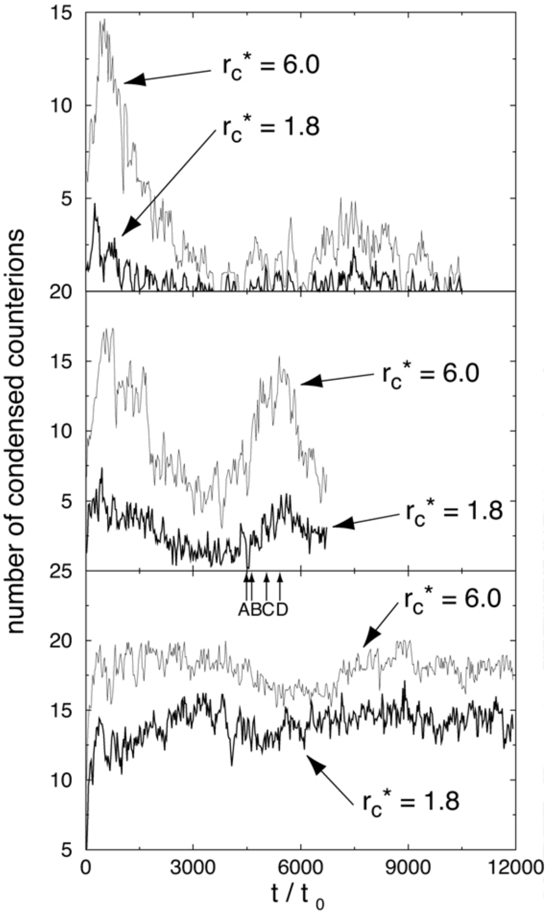

Fig. 5. Time evolution of the number of condensed counterions for $q^* = 1.2$, 2.4 and 6.0 (from top to bottom) using a condensation criterion $r_c^* = 1.8$ (thick solid line) and $r_c^* = 6.0$ (thin solid line). For $q^* = 2.4$, the arrows represent the time location of the four translocation stages (A, B, C, and D) presented in Fig. 7.

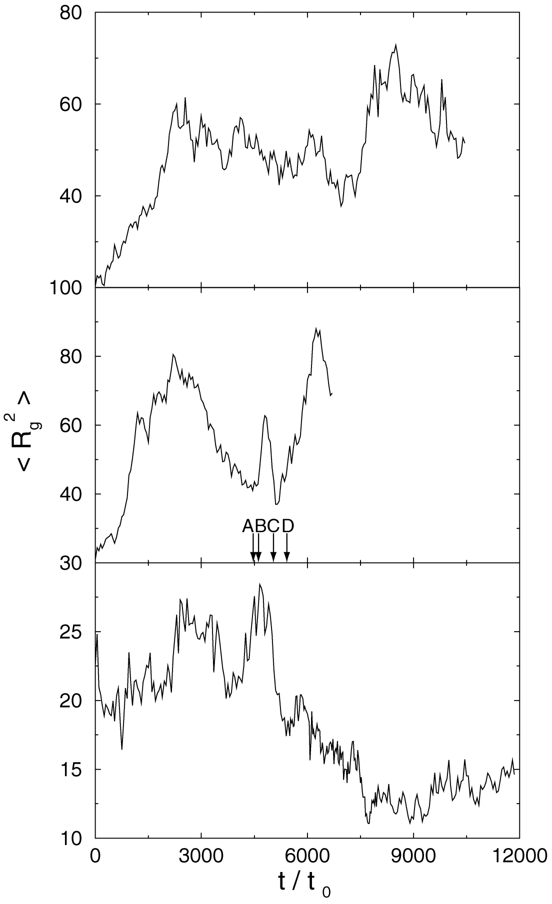

Fig. 6. Time evolution of the mean square radius of gyration $\langle R_g^2 \rangle$ for $q^* = 1.2$, 2.4 and 6.0 (top to bottom). For $q^* = 2.4$, the arrows represent the time location of the four translocation stages (A, B, C, and D) presented in Fig. 7.

the counterion binding to the polymer. Average values for the number of condensed counterions under external electric field are given in Table 1.

The main qualitative features exhibited during the time evolution are independent of the chosen value for r_c^*. Fig. 5 shows the time evolution of the number of condensed counterions for the three systems for $r_c^* = 1.8$ and 6.0. The $q^* = 6.0$ system does not exhibit any significant changes in the number of condensed counterions over the duration of the simulation. The counterions are mostly condensed on the chain, and the electric field slightly enhances this effect. By contrast, for the $q^* = 1.2$ system, a strong decrease in the number of condensed counterions occurs in an external field, the new equilibrium configuration being reached after a time $t^* \simeq 2500$. The $q^* = 2.4$ system exhibits an initial decrease in the number of counterions induced by the external electric field similar to that for $q^* = 1.2$ with a new equilibrium state also reached after a duration $t^* \simeq 2500$. This effect is weaker, however (see Table 1 and Fig. 4) due to the fact that a larger fraction of counterions are condensed on the chain ($q_c^* < q^* = 2.4$). The behavior during the translocation process is discussed in Section 3.2.

We turn now to the study of the polymer conformations as a function of magnitude of the site charge q^* and electric field E^*. A global measure of the polymer conformation is the mean square radius of gyration R_g^2, defined as:

$$R_g^2 = \frac{1}{N} \sum_{i=1}^{N} \langle (\mathbf{r}_i - \mathbf{R})^2 \rangle \qquad (6)$$

where $\mathbf{r}_i$ is the position of the ith polymer site, N is the number of sites in the chain, and $\mathbf{R}$ is the position of the center of mass of the chain. Average values of R_g^2 over a duration $t^* = 2500$ for the three systems with and without applied electric field are listed in Table 1. Fig. 6 shows the time evolution of R_g^2 for $q^* = 1.2$, 2.4 and 6.0. For $q^* = 1.2$, the chain becomes more elongated under the action of the external field because the mobile counterions are stripped away by the field, leaving the bare negative ions on the polymer and leading to an electrostatic stiffening of the polymer. For $q^* = 2.4$, the first effect of the electric field, before translocation through the pore, is to strip away the fraction of counterions which are in the potential trough of the polymer, resulting in a loss of electrostatic screening of the negative charges on the polymer and an increase in R_g^2. Then the polymer chain is driven through the reservoir by the electric field and pushed against the lower substrate (Fig. 2). Conformational changes during the translocation process are discussed in Section 3.2.

For $q^* = 6.0$, the radius of gyration is of the same order of magnitude as for $q^* = 1.2$ and 2.4 when no external field is applied. Under an external electric field, no significant change in the magnitude of the radius of gyration is observed over a time interval $t^* \simeq 5000$, then a strong decrease in R_g^2 occurs, indicative of the tightly collapsed structure adopted by the chain (Fig. 6). Additional studies are needed to determine whether the observed collapse is induced by the external field or is simply caused by strong counterion condensation. Biological processes and theoretical works tend to favor the latter hypothesis. The chain collapse is analogous to the packing of DNA into a cell [25]. This packing requires overcoming an enormous Coulombic barrier in a highly dilute aqueous solution containing a small concentration of polvalent cations. Simulations and theory have demonstrated short-range attraction between two macroions modeled as charged cylinders [26,27] or stiff polymers [28]. This attraction has been ascribed to correlated fluctuations of the counterions induced by counterion condensation [29,30]. Self-attraction have been shown to occur also in flexible polyelectrolytes [31–34]. Theoretical work using simple scaling arguments have shown that counterion condensation modifies the second virial coefficient of a polyelectrolyte due to the fact that at low enough temperature (or at high enough counterion valence) the counterions approach close enough to the macroion to form dipoles, leading to charge–dipole and dipole–dipole interactions [32,35]. Similar ideas have been developed by Brilliantov et al. [33], who also predict also a first order phase transition between a stretched polyelectrolyte and a strongly collapsed polyelectrolyte as a function of magnitude of electric charges due to counterion condensation.

3.2. Translocation process

The thermodynamics of electrophoresis in the presence of a narrow pore is complex and involves traversal of entropic and enthalpic barriers [3,4,36–43]. When the chain enters the pore, its conformational entropy is reduced, due to chain elongation. On the other hand, due to the small size of the pore aperture a significant fraction of the counterions are stripped from the chain and gain configurational entropy. The counterion unbinding also results in an increase in the Coulombic energy. In addition, the electrostatic energy of interaction of the macroion with the external field decreases as the negatively charged chain moves through the pore, and the electrostatic interaction energy of the free counterions also decreases. The situation is reversed when the polymer exits the pore. However, the gain in conformational entropy of the polymer upon exiting the pore is probably greater than the entropy loss associated with pore entry, since before pore entry the polymer is pushed against the lower substrate surface ($z = -z_0$) and behaves like a conformationally restricted two-dimensional chain while it behaves like a three-dimensional chain upon exiting the pore. Detailed free energy calculations are needed to study the importance of these contributions in the translocation process. We focus here on the kinetics of the translocation process under a large electric field.

Translocation was only observed in the $q^* = 2.4$ simulation. As we have seen in Section 3.1, for $q^* = 6.0$, strong counterion condensation results in repulsive screened Coulomb interactions between the ions on the chain and self-attraction due to charge–dipole, dipole–dipole interactions and/or charge fluctuation along the chain. In the $q^* = 6.0$ system, the chain adopts a collapsed structure with an effective diameter larger than the pore diameter, effectively preventing translocation. There is, a priori, no reason for the $q^* = 1.2$ system not to translocate since the chain adopts an extended conformation. The simulation has to be performed over a long enough period of time to permit the polymer to find the pore entrance via diffusion along the substrate surface.

Due to the large external field, translocation of the polymer in the $q^* = 2.4$ system occurs after a short drift time spent in the reservoir. The polymer finds the entrance of the pore after a time interval $\Delta t^* = 4000$ ($\Delta t = 2.8$ ns) after application of the field. The upper part of Fig. 7 shows several stages in the translocation process. For clarity, only the polymer chain and the counterions are shown. The translocation starts when the first bead (head) enters the pore at $z = -z_0$ and ends when the last bead (tail) exits the pore at $z = z_0$. The total translocation process occurs over a period of time $\Delta t^* \simeq 950$, corresponding to 0.665 ns. A movie of the polymer translocation is available at: http://flcmrc.colorado.edu/theme3.html.

Timescales reported for translocation of ions and water molecules are in the range 10^{-6}–10^{-9} s, in reasonable agreement with our results.

We have decomposed the translocation process into three stages [37] in which the conformation of the polymer and its interactions with the pore are significantly different: the first stage corresponds to the translocation of the head from the entrance to the exit of the pore, the second stage corresponds to the exit of the head from the pore and the translocation of the tail from the reservoir to the entrance of the pore, and the third stage corresponds to the translocation of the tail from the entrance to the exit of the pore (see Fig. 7). The duration of each stage of translocation is: $\Delta t_1^* = t_{z=z_0}^{\text{head}} - t_{z=-z_0}^{\text{head}} = 145.74$ ($\Delta t_1 = 0.102$ ns); $\Delta t_2^* = t_{z=-z_0}^{\text{tail}} - t_{z=z_0}^{\text{head}} = 424.75$ ($\Delta t_2 = 0.297$ ns) and $\Delta t_3^* = t_{z=z_0}^{\text{tail}} - t_{z=-z_0}^{\text{tail}} = 379$ ($\Delta t_3 = 0.266$ ns). The duration of the second and third stages are comparable, but are nearly three times as long as the first stage. These differences in time are probably due to variation in the

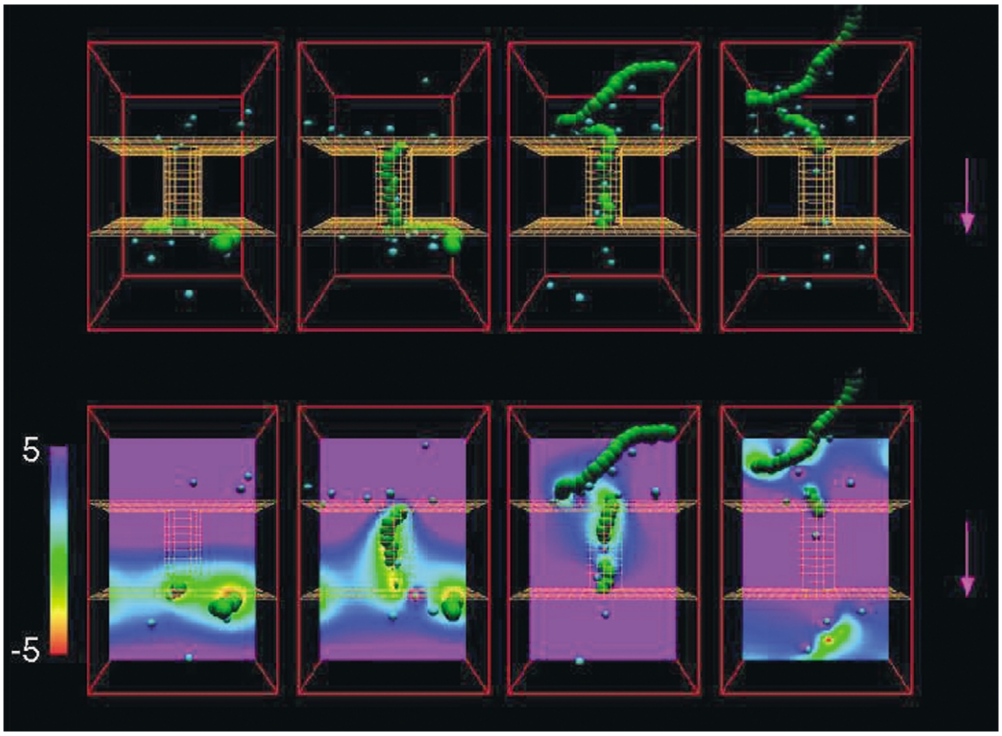

Fig. 7. Top: Four stages in the translocation process, from left to right: head of the polymer at the entrance of the pore ($t^* = 4472.75$), head at the exit of the pore ($t^* = 4618.5$), tail at the entrance ($t^* = 5043.25$), tail at the exit ($t^* = 5422.25$). Bottom: Corresponding reduced electrostatic potential $V^* = V/V_0$ ($V_0 = \epsilon_0/q_0$) produced by the charge distribution in the plane (xz) passing through the center of the pore. Values of the potential outside the range chosen $(-5, +5)$ are assigned to the colors corresponding to the minimum and maximum values, and for clarity the water molecules have not been represented.

magnitude of the total electric field $E^*_{\text{total}} = E^* + E^*_{\text{int}}$ experienced by the polymer during the translocation, where E^*_{int} is the internal field induced by the charge distribution.

The bottom part of Fig. 7 shows the reduced electrostatic potential $V^* = V/V_0$ ($V_0 = \epsilon_0/q_0$) due to ions and counterions in the (xz) plane passing through the middle of the pore. We clearly see an inversion in the sign of the potential difference across the pore during the second stage of polymer translocation due to a change in the relative charge density on the two substrate surfaces. This change leads to an inversion in the direction of the internal field E^*_{int}, which in turn slows down the translocation process. The upper and lower substrate surfaces behave like a capacitor, with an excess of positive charges on the upper surface—the free counterions trying to translocate and pushed against the surface by the external electric field—and an excess of negative charges on the lower surface—the polymer chain wandering at the pore entrance. This situation is reversed when enough negatively charged monomers have translocated, analogous to the discharge of a capacitor.

Fig. 8 shows quantitatively the time evolution of the reduced internal electric field E^*_{int}, defined as $E^*_{\text{int}} = \Delta V^*_{\text{pore}}/l^*_{\text{pore}}$, across the pore during the translocation event, with ΔV^*_{pore} being the average potential difference across the pore defined as $\Delta V^*_{\text{pore}} = 1/4\sum_{i=1}^{4} \times (V^*(x_i, y_i, -z_0) - V^*(x_i, y_i, z_0))$ with $(x_i = 0; y_i = \pm r_0)$ for $i = 1, 2$ and $(x_i = \pm r_0; y_i = 0)$ for $i = 3, 4$ (see Fig. 1). It confirms that the internal field decreases in magnitude and changes sign when the middle of the chain crosses the middle of the pore (i.e. in the second stage) resulting in a smaller magnitude of total electric field E^*_{tot} and a slower translocation process.

We turn now to the identification of single translocation events involving either a counterion or charged sites on the polymer. In order to mimic the signal recorded at the gate of a transistor located on the inner cylindrical surface of the

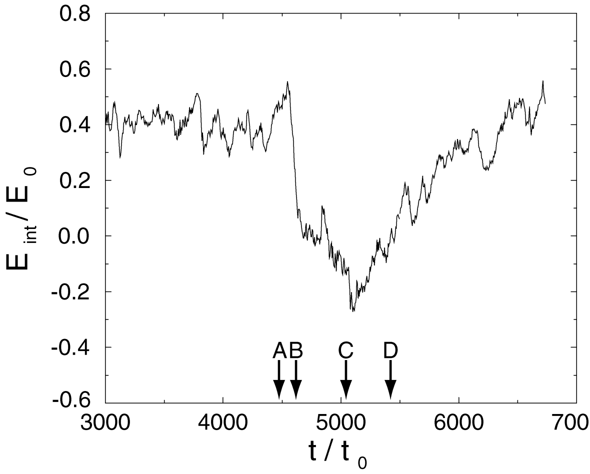

Fig. 8. Time evolution of the induced electric field E^* produced by the distribution of charges. The arrows represent the time location of the four translocation stages presented in Fig. 7.

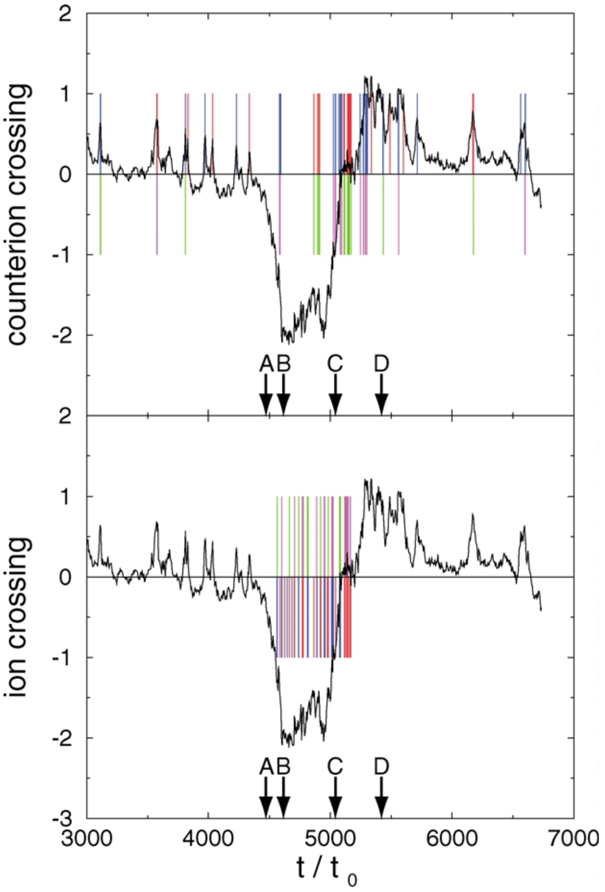

Fig. 9. Time evolution of the reduced electrostatic potential V^* and of the events corresponding to the passage of counterions (top) and ions (bottom) through the midplane of the pore ($z = 0$), during polymer translocation. A positive peak corresponds to an ion or counterion passing in the same direction as the field while a negative peak corresponds to an ion or counterion passing in opposite direction.

pore, we have computed the electrostatic potential V^* at four equidistant positions ($x = 0; y = \pm r_0$) and ($x = \pm r_0; y = 0$) on the surface of the mid-plane ($z = 0$) of the pore. We have simultaneously recorded events corresponding to the passage of charged sites (either counterions or charged polymer beads) through the $z = 0$ plane to investigate the correlations between signal and site positions. Fig. 9 shows the time evolution of V^* averaged over the four sensors as well as ion passage events during the translocation process. A positive spike records the passage of a charge in the same direction as the external electric field while a negative spike records the passage of a charge in the opposite direction. No counterions are pulled into the pore with the polymer so we do not have any counterions translocating against the electric field direction during polymer translocation. A strong correlation is found between counterion positions and the signal (sharp peaks in V^*). It is also fairly easy to detect when the polymer translocation takes place (and its approximate duration), but the discrimination of individual charges on the polymer chain is more problematic due mainly to the small separation between neighboring charged sites on the chain, fluctuations in chain position, and the simultaneous translocation of counterions. Further analysis or filtering of the signal is required to achieve single-ion discrimination even with this simple model.

We notice that a significant larger number of counterions find the entrance of the pore during the third stage of polymer translocation. During the translocation process, the number of condensed counterions on the chain increases significantly (Fig. 5). Due to the applied electric field, an excess counterion density is located near the upper substrate surface and a significant fraction of them—the ones near the aperture—condense back onto the polymer as soon as the head of the chain exits the nanopore (see Fig. 7). The condensed counterions near the tail of the polymer are relatively mobile and have a significant probability of being stripped from the chain due to the external field and friction with the solvent molecules. The translocation of these counterions is facilitated by the polymer, which acts as a guide to the pore entrance.

In addition, the head of the polymer exiting the nanopore during the translocation process experiences a stronger electric field than inside the pore (see above). The polymer tail is still pushed by the field against the lower substrate surface creating an anchoring point on the substrate (see Fig. 7) while the head of the chain is stretched by the electric field at the pore exit. This effect results in an increase in R_g^2 (Fig. 6). After the head has exited the pore, counterion condensation back on the head, screening the Coulombic interactions and reducing the stretching force, as well as a weaker anchoring at the entrance of the pore due to the presence of fewer monomers, are responsible for the decrease in polymer extension, the chain behaving like a rubber band. As the translocation proceeds, the tail enters the pore and the release of the anchoring point induces a significant contraction of the chain.

4. Conclusions

Using a coarse-grained bead-spring model, we have studied the electrophoretic translocation of a charged polymer through a nanopore for various charge magnitudes under the application of an external electric field. Three regimes can be identified, corresponding to drift of the polymer in the reservoir, diffusion of the polymer along the substrate surface in search of the pore entrance and polymer translocation through the pore. The three systems studied, with reduced charges, $q^* = 1.2$, 2.4 and 6.0, respectively, exhibit counterion condensation when no electric field is applied, but the $q^* = 1.2$ system presents a much less strongly bound macroion–counterion complex than the other two. Counterion condensation leads to significant changes in polymer conformation, with a rather extended chain conformation for $q^* = 1.2$ and a collapsed chain conformation for $q^* = 6.0$, due to self-attraction induced by charge–dipole/dipole–dipole interactions and/or counterion fluctuations along the chain. An external electric field can strip the counterions from the chain, depending on the relative magnitude of the field and the charge of the ions and counterions, inducing significant changes in polymer conformation. Due to the strong external electric field used, translocation occurs quickly for the $q^* = 2.4$ system. By contrast, translocation in the $q^* = 6$ system is inhibited due to the collapsed conformation adopted by the chain. The rate of polymer translocation is not constant over the entire process. Specifically, the chain translocates more slowly after its midpoint crosses the mid-plane of the pore due to an inversion in the direction of the internal electrostatic field produced by the time-varying distribution of charges. The upper and lower substrate surfaces behave qualitatively like a capacitor, which undergoes a discharge. By recording the electrostatic potential, we were able to identify the passage of individual counterions unambiguously. However, it is difficult to identify translocation events involving single charged sites on the polymer due mainly to the small distance between neighboring ions, fluctuations in polymer position, and simultaneous counterion translocation.

This work is exploratory and many questions remain unanswered. Future work will focus on both the translocation phenomenon and on bulk electrophoresis. Using the simple model presented in this work, we will study the electrophoresis process in detail, including the effect of external electric field on counterion condensation as a function of the ion charge magnitude and macroion concentration. Special emphasis will be given to the modification of macroion conformation induced by the external field. In the framework of the simple model introduced in this study, we will study the translocation process statistically by steering the polymer through the pore and performing free energy computations to assess the relative importance of entropic and enthalpic contributions to the free energy of pore traversal.

References

[1] Kasianowicz JJ, Brandin E, Branton D, Deamer DW. Characterization of individual polynucleotide molecules using a membrane channel. Proc Natl Acad Sci USA 1996;93:13770–3.

[2] Bokhari SH, Glaser MA, Jordan HF, Lansac Y, Sauer JR, Van Zeghbroeck B. IEEE Computer Society Bioinformatics Conference (Stanford University, Palo Alto, CA, 14–16 August); 2002. p. 291–302.

[3] Muthukumar M. Polymer translocation through a hole. J Chem Phys 1999;111:10371–4.

[4] Muthukumar M. Translocation of a confined polymer through a hole. Phys Rev Lett 2001;86:3188–91.

[5] Kong CY, Muthukumar M. Modeling of polynucleotide translocation through protein pores and nanotubes. Electrophoresis 2002;23: 2697–703.

[6] Parsegian A. Energy of ion crossing a low dielectric membrane: solutions to four relevant electrostatic problems. Nature 1969;221: 844–6.

[7] Zimm BH, Levene SD. Problems and prospects in the theory of gel-electrophoresis of DNA. Q Rev Biophys 1992;25:171–204.

[8] Baschnagel J, Binder K, Paul W, Laso M, Sutter UW, Batoulis I, Jilge W, Bürger T. On the construction of coarse-grained models for linear flexible polymer chains: distribution functions for groups of consecutive monomers. J Chem Phys 1991;95:6014–25.

[9] Murat M, Kremer K. From many monomers to many polymers: soft ellipsoid model for polymer melts and mixtures. J Chem Phys 1998; 108:4340–8.

[10] Schweizer KS, David EF, Singh C, Curro JG, Rajasekaran JJ. Structure–property correlations of atomistic and coarse-grained models of polymer melts. Macromolecules 1995;28:1528–40.

[11] Tschöp W, Kremer K, Batoulis J, Bürger T, Hahn O. Simulation of polymer melts. I. Coarse-graining procedure for polycarbonates. Acta Polym 1998;49:61–74.

[12] Johnson JK, Zollweg JA, Gubbins KE. The Lennard–Jones equation of state revisited. Mol Phys 1992;78:591–618.

[13] Tournier AL, Huang D, Schwarzl SM, Fisher S, Smith JC. Time-resolved computational protein biochemistry: solvent effects on interactions, conformational transitions and equilibrium fluctuations. Faraday Discuss 2002;122:243–51.

[14] Mamonov AB, Coalson RD, Nitzan A, Kurnikova MG. The role of the dielectric barrier in narrow biological channels: a novel composite approach to modeling single-channel currents. Biophys J 2003;84: 3646–61.

[15] Berendsen HJC, Postma JPM, van Gunsteren WF, Dinola A, Haak JR. Molecular dynamics with coupling to an external bath. J Chem Phys 1984;81:3684–90.

[16] Darden T, York D, Pedersen L. Particle mesh Ewald: an N log N method for Ewald sums in large systems. J Chem Phys 1993;98: 10089–92.

[17] Essmann U, Perera L, Berkowitz ML, Darden T, Lee H, Pedersen LG. A smooth particle mesh Ewald method. J Chem Phys 1995;103: 8577–93.

[18] Ewald PP. Die Berechnung optischer und elektrostatisher Gitter-potentiale. Ann Physik 1921;64:253.

[19] Toukmaji AY, Board Jr JA. Ewald summation techniques in perspective: a survey. Comput Phys Commun 1996;95:73–92.

[20] Manning GS. Limiting laws and counterion condensation in polyelectrolyte solutions. 7. Electrophoretic mobility and conductance. J Phys Chem 1981;85:1506–15.

[21] Fuoss RM, Accascina F. Electrolytic conductance. New York: Interscience; 1959.

[22] Oosawa F. Polyelectrolytes. New York: Marcel Dekker; 1971.

[23] Manning GS. Molecular theory of polyelectrolyte solutions with applications to electrostatic properties of polynucleotides. Q Rev Biophys 1978;11:179–246.

[24] Tanaka M, Grosberg AYu. Electrophoresis of a charge–inverted macroion complex: molecular-dynamics study. Eur Phys J E 2002;7: 371–9.

[25] Bloomfield VA. DNA condensation. Curr Opin Struct Biol 1996;6: 334–41.

[26] Gronbech-Jensen N, Mashl RJ, Bruinsma RF, Gelbart WM. Counterion-induced attraction between rigid polyelectrolytes. Phys Rev Lett 1997;78:2477–80.

[27] Lyubartsev AP, Nordenskiöld L. Monte Carlo simulation study of polyelectrolyte properties in the presence of multivalent polyamine ions. J Polym Chem B 1995;101:4335–42.

[28] Stevens MJ. Bundle binding in polyelectrolyte solutions. Phys Rev Lett 1999;82:101–4.

[29] Ha BY, Liu AJ. Counterion-mediated attraction between two like-charged rods. Phys Rev Lett 1997;79:1289–92.

[30] Manning GS, Ray J. Fluctuations of counterions condensed on charged polymers. Langmuir 1994;10:962–6.

[31] Stevens MJ, Kremer K. The nature of flexible linear polyelectrolytes in salt free solution: a molecular dynamics study. J Chem Phys 1995; 103:1669–90.

[32] Schiessel H, Pincus P. Counterion-condensation-inducedcollapse of highly charged polyelectrolytes. Macromolecules 1998;31:7953–9.

[33] Brilliantov NV, Kuznetsov DV, Klein R. Chain collapse and counterion condensation in dilute polyelectrolyte solutions. Phys Rev Lett 1998;81:1433–6.

[34] Winkler RG, Gold M, Reineker P. Collapse of polyelectrolyte macromolecules by counterion condensation and ion pair formation: a molecular dynamics simulation study. Phys Rev Lett 1998;80:3731–4.

[35] Kuhn PS. A simple model for the collapse of polyelectrolytemacromolecules. Physica A 2002;311:50–8.

[36] Ambjörnsson T, Apell SP, Konkoli Z, Di Marzio EA, Kasianowicz JJ. Charged polymer membrane translocation. J Chem Phys 2002;117: 4063–73.

[37] Slonkina E, Kolomeisky AB. Polymer translocation through a long nanopore. J Chem Phys 2003;118:7112–8.

[38] Lubensky DK, Nelson DR. Driven polymer translocation through a narrow pore. Biophys J 1999;77:1824–38.

[39] Sung W, Park PJ. Polymer translocation through a pore in a membrane. Phys Rev Lett 1996;77:783–6.

[40] Boehm RE. Steady-state permeation rate of homopolymer chain molecules through a pore in a barrier. Macromolecules 1999;32: 7645–54.

[41] Sebastian KL, Paul AKR. Kramers problem for a polymer in a double well. Phys Rev E 2000;62:927–39.

[42] Kumar KK, Sebastian KL. Adsorption-assisted translocation of a chain molecule through a pore. Phys Rev E 2000;62:7536–9.

[43] Lee S, Sung W. Coil-to-stretch transition, kink formation, and efficient barrier crossing of a flexible chain. Phys Rev E 2001;63: 021115.